Multi-enzyme co-immobilization on tri-heterofunctional supports

Javier Santiago-Arcos[a]‡, *Susana Velasco-Lozano*[a,b,c]‡* *and Fernando López-Gallego*[a,d]*

[a] Heterogeneous Biocatalysis group, CIC biomaGUNE, Edificio Empresarial "C", Paseo de Miramón 182, 20009, Donostia, Spain.
[b] Instituto de Síntesis Química y Catálisis Homogénea (ISQCH-CSIC), Universidad de Zaragoza, C/ Pedro Cerbuna, 12, 50009, Zaragoza, Spain.
[c] Aragonese Foundation for Research and Development (ARAID), Zaragoza (Spain)
[d] IKERBASQUE, Basque Foundation for Science, Bilbao (Spain)
‡Equal contribution.

*Corresponding authors. (F. López-Gallego) and (S. Velasco-Lozano)
Phone: +34 943003500 Ext 309, Fax: +34 943003501
E-mail addresses: flopez@cicbiomagune.es and svelasco@unizar.es

KEYWORDS: co-immobilization, multi-enzyme systems, heterogeneous-activated supports, enzyme stabilization.

ABSTRACT

Multi-enzyme cascade biotransformations in one pot are gaining momentum since they have demonstrated enhanced catalytic performance than traditional step-by-step transformations requiring sequential pots. Although their evident advantages, the co-immobilization of several enzymes requiring different anchoring chemistries and stability conditions is still challenging. In this work, we exploited an heterofunctional support activated with three different chemical functionalities in order to immobilize a wide variety of different enzymes under mild conditions.

This support is based on agarose microbeads activated with aldehyde, amino and cobalt-chelates moieties that allow a fast and irreversible immobilization of enzymes (5 to 30 min), making most of the heterogeneous biocatalysts highly thermostable (up to 21-fold higher than the soluble one). We also demonstrated the potential of this tri-functional support to efficiently co-immobilize a multi-enzyme system composed by an alcohol dehydrogenase, a NADH oxidase and a catalase. The confined multi-enzymatic system demonstrates higher performance than the soluble enzyme counterparts reaching and accumulated TTN of $1x10^4$ during five batch consecutive cycles under operational conditions. Finally, we expanded the versatility of the described exploited heterogeneous chemistry to other frequently used immobilization supports such as cellulose microbeads and commercial methacrylate porous beads. We envision this solid material to be a reference platform for co-immobilizing multi-enzyme systems with enhanced properties to catalyze stepwise biotransformations.

Introduction

Enzyme immobilization is a well spread and capitalized technique exploited in a broad variety of biocatalytic industrial applications such as drug development, chemical synthesis, energy and fuels production, polymer synthesis, biomedicine and biosensors, food and cosmetics.[1] Confined in a defined space, immobilized enzymes remain as heterogeneous biocatalyst in the reaction mixture, thus simplifying its separation and recycling.[2] Beyond these advantages, enzyme immobilization has been extensively employed to enhance enzyme stability[3, 4, 5] and to control/modulate enzyme catalytic properties.[6] During the last 50 years, separately immobilized enzymes have been the most reported ones, whereas Systems Biocatalysis is encouraging new efforts to immobilize several enzymes on the same particle (co-immobilization) to finally create artificial biosynthetic routes.[7]

Multi-step biocatalysis allows running enzyme cascades into one-pot reaction systems, which compared with multi-pot cascade approaches, minimizes the reaction steps, reduces the by-product formation, decreases the accumulation of toxic or unstable intermediates, shift the thermodynamic equilibrium toward the target product, in situ recycling of enzyme cofactors if required, and ultimately increases the productivity, the titer and the cost-efficiency of the bioprocess.[8] However, cascade biotransformations must overcome several obstacles related to the different stability and reactivity requirements of each enzyme forming the system.[9] Enzyme co-immobilization is a recurrent strategy to solve some of these drawbacks ideally providing a suitable compartmentalized microenvironment where the enzymes may be spatially organized at the right density to increasing the overall cascade efficiency, easing reaction work-ups and enabling the biocatalyst reutilization.[10] However, the co-immobilization of two or more enzymes on the same support is not trivial as one immobilization strategy might be beneficial for one enzyme but detrimental for the other(s). Therefore, co-immobilization by itself does not guarantee the activity and stability of an heterogeneous multi-enzyme system.[11] In this context, heterofunctional supports activated with more than one reactive group emerge as an excellent solution to co-immobilize multi-enzyme systems on the same surface where each enzyme is attached to the support through its optimal immobilization chemistry. The vast majority heterofunctional supports offer the combination of only two reactive groups; one (i.e ionic, hydrophobic, metal chelate groups) to drive the enzyme adsorption, and the other (i.e epoxy, aldehyde, glyoxyl and vinyl groups) to react with the exposed nucleophilic residues on the enzyme surface to form covalent and irreversible bonds.[12, 13] The combination of these two groups allows a two-step enzyme immobilization, in which the enzyme is first absorbed very quickly to the support (close contact), and then irreversible covalent attachment between the enzyme and the support are formed.[14] Although heterofunctional

supports have been mainly harnessed to accomplish the multivalent covalent immobilization of single-enzymes at mild conditions, recent trends are more focused on their use as a chassis for the co-immobilization of multi-enzyme systems controlling their spatial organization.[11, 15]

In this work, we have exploited and characterized porous supports functionalized with three reactive groups; metal-chelates to site-directed immobilized His-tagged enzymes, positively charged amines to ionically absorb them and electrophile groups (aldehydes or epoxides) to promote their multivalent covalent attachment to the support surface (Scheme 1a-b). A similar tri-functional support was reported for the immobilization of a sole enzyme but never intended for the co-immobilization of a multi-enzyme system.[16] We immobilized a pallet of six different enzymes on this tri-functional support and characterized their immobilization kinetics, stability and structural rearrangements upon the immobilization process. To demonstrate the potential of this tri-functional support for the co-immobilization of multi-enzyme systems, we challenged it with a model system composed of three enzymes that orthogonally work to selectively oxidize 1,5 pentanodiol into its corresponding lactol with *in situ* NAD^+ regeneration and H_2O_2 removal (Scheme 1c).[17] Finally, we evaluated the stability and reusability of the co-immobilized enzyme preparations in a batch reactor operated for consecutive and discontinuous reaction cycles.

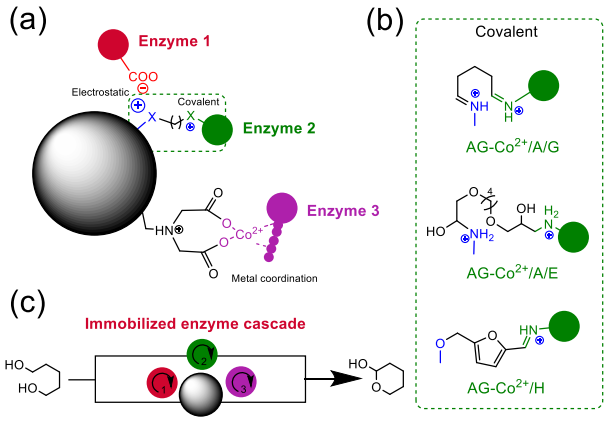

Figure 1. (a) Surface of a tri-functional support that co-immobilizes several enzymes through three different immobilization chemistries. (b) Chemical scheme of the different electrophiles that covalently bind enzymes. (c) One-pot oxidation of 1,5-pentanodiol into 2-Tetrahydropyranol catalyzed by a three-enzyme cascade co-immobilized on the trifunctional support described in panel (a).

Experimental methods

Materials

The enzymes alcohol dehydrogenase from *Bacillus stearothermophilus* (BsADH), NADH oxidase from *Thermus thermophilus HB27* (TtNOX), catalase from *Bordetella pertussis* (BpCAT) and the lactonase from *Sulfolobus islandicus* (SiLAC) were produced as previously reported.[18] 4% cross-linked agarose beads (AG) were purchased from Agarose Bead Technologies (Madrid, Spain), epoxy methacrylate microbeads ECR8204F (Pu) were kindly donated by Purolite®, Cellulose MT200 was purchased from IONTOSORB (Usti and Labem, Czech Republic). Compounds as ethylenediamine, imidazole, iminodiacetic acid, cobalt chloride, sodium periodate, sodium hydroxide fluorescein isothiocyanate (FITC), rhodamine B isothiocyanate, sodium acetate, sodium chloride, sodium phosphate, sodium bicarbonate, glutaraldehyde, SYPRO Orange Protein Gel Stain, 1,5-pentanediol, 5-hydroxypentanal, tetrahydro-2H-pyran-2-ol, δ-valerolactone, as well as the enzymes catalase from bovine liver (BlCAT) and alcohol dehydrogenase from horse liver

(HlADH) were acquired from Sigma-Aldrich Chemical Co. (St. Louis, IL, USA). All other reagents were of analytical grade.

Preparation of tri-heterofunctional support activated with cobalt-chelates, secondary amine groups and aldehydes (AG-Co^2/A/G)

For the first step we prepared epoxy-activated agarose (AG-E) as described elsewere.[13] Then, we activated the AG-E with iminodiacetic acid (AG-E/IDA) by preparing a suspension of 10 g (≈ 14 mL) of AG-E in 100 mL of 0.5 M iminodiacetic acid at pH 11. The suspension was maintained under gentle agitation at 200 rpm for 1 h at room temperature (RT). Afterwards, the support was filtered and rinsed with 10 volumes of water. Once AG-E/IDA was obtained, we introduced amino groups by incubating it over night with 10 volumes of 2 M ethylenediamine at pH 11 (AG-A/IDA) under gentle agitation at 200 rpm at room temperature. Later, the support was filtered and gently rinsed with water. Then, the introduction of aldehyde moieties was conducted by incubating the support over night with 15% glutaraldehyde solution in 200 mM sodium phosphate buffer pH 7 (AG-IDA/A/G) under gentle agitation at 200 rpm at room temperature. Once the incubation concluded, the support was filtered and washed with at least 10 volumes of water. Finally, to introduce the metal group, the support was incubated with 10 volumes of 30 $mg \cdot mL^{-1}$ $CoCl_2$ during 2 h at room temperature (AG-Co^{2+}/A/G). At the end, the support was filtered and washed with abundant water and stored at 4 ºC protected from light (Supplementary, Scheme S1).

Preparation of tri-heterofunctional support activated with cobalt-chelates, secondary amine groups and epoxides (AG-Co^{2+}/A/E)

1 volume of AG-A/IDA was suspended in 20 volumes of 0.15 M 1,4-butanediol diglycidyl ether (BD), 12% acetone in 80 mM bicarbonate buffer pH 9 and incubated over night under gentle agitation at 200 rpm at room temperature. Once the incubation concluded, the support was filtered and washed with at least 10 volumes of 20% acetone in water, and then with only water. Finally, to introduce the metal group, the support was incubated with 10 volumes of 30 mg·mL^{-1} $CoCl_2$ during 2 h, at room temperature (AG-Co^{2+}/A/E). At the end, the support was filtered and washed with abundant water and stored at 4 ºC protected from light (Supplementary, Scheme S2).

Preparation of bi-heterofunctional support activated with cobalt chelates and hydroxymethyl furfural AG-Co^{2+}/H

1 volume of AG-E/IDA was suspended in 10 volumes of 100 mM hydroxymethylfurfural (HMF), in 100 mM sodium phosphate buffer pH 8 and incubated over night under gentle agitation at 200 rpm at RT (AG-H/IDA). Once the incubation concluded, the support was filtered and washed with at least 10 volumes of water. Finally, to introduce the metal ligand, the support was incubated with 10 volumes of 30 mg·mL^{-1} $CoCl_2$ during 2 h, at room temperature (AG-Co^{2+}/H). At the end, the support was filtered and washed with abundant water and stored at 4 ºC protected from light (Supplementary, Scheme S3).

Preparation of tri-heterofunctional supports CEL-Co^{2+}/A/G and Pu-Co^{2+}/A/G

The functionalization of cellulose-microbeads (CEL) and polymethacrylate-microbeads (Pu) were done following the same activation protocol to prepare AG-Co^{2+}/A/G but replacing AG by CEL (CEL-Co^{2+}/A/G) or Pu microbeads (Pu-Co^{2+}/A/G). While the Pu microbeads are commercially

supplied with epoxides (ECR8204F), cellulose was activated with the epoxy groups following the same protocol as for agarose.[13]

Degree of activation of the supports

Epoxy groups quantitation

Epoxy groups were quantified indirectly through the oxidation of the diols resulting from epoxide ring opening under acid conditions. These diols were then titrated with $NaIO_4$ as described elsewhere. [19] Briefly, 1 g of the support was incubated with 10 mL of 0.5 M H_2SO_4 for 1 h at room temperature in order to hydrolyze the epoxy groups. Afterwards, the hydrolyzed support (yielding vicinal diols) was oxidized with 10 mM $NaIO_4$ (1:10 suspension) by incubation at room temperature (typically 1-2 hours). The number of epoxy groups was calculated by the difference in $NaIO_4$ consumption between the hydrolyzed support and the initial epoxy support. Different consumption degree of periodate was quantified by titration with potassium iodide (KI). Briefly, 20 µL of remnant $NaIO_4$ in the supernatant were mixed with 200 µL of 10% KI in saturated bicarbonate solution and measuring the absorbance at 405 nm.

IDA groups quantitation

IDA groups were indirectly quantified following the same hydrolysis procedure as for epoxy groups quantitation, but hydrolysing both AG-IDA/E and AG-E with H_2SO_4 for 1 h at room temperature in order to hydrolyze the epoxy groups. Once epoxy groups were hydrolyzed, the formed diols were measured by oxidative titration with $NaIO_4$. IDA groups were calculated as the difference in $NaIO_4$ consumption of hydrolyzed both AG-E (before IDA groups introduction) and

AG-IDA/E. The consumption of periodate was spectrophotometrically measured by titration with KI as previously described.

Amino groups quantitation

Introduced amino groups were quantified by titration with picrylsulfonic acid.[20] Briefly, 0.25 mL of picrylsulfonic acid solution (5% w/v) diluted 500 times in 100 mM sodium bicarbonate buffer pH 8.5 (Cat. P2297 Sigma-Aldrich) were mixed with 0.5 mL of a suspension 1:10 of AG-IDA/A in 100 mM sodium bicarbonate buffer pH 8.5. The mixture was incubated at 37 ºC during 2 h with gentle mixing. Afterwards, the support was washed 4 times with 0.75 mL of 1 M NaCl followed by 5 washes of 0.75 mL of distilled water. The washed support was resuspended 1:10 in distilled water in order to measure the absorbance of 200 µL at 335 nm against a support control without amino functionalization (AG-IDA/E). Calibration curve of ethylenediamine (linear range 0.03 – 0.25 mM) was also prepared under the same conditions. Micrographs of the picrylsulfonic activated AG-IDA/E were acquired by placing 100 µL of a 1:200 water suspension of the support in water in a 96-well clear bottom black microplate and visualized using a Plan Fluorite 4X phase objetive and performed color brightfield imaging, multicolored LED illumination within a Cytation5 Cell Imaging Reader (BioTek Instruments) (Supplementary, Figure S1B).

Aldehyde groups quantitation

Aldehyde functionalization with glutaraldehyde was quantified by titration with Schiff's reagent.[21] Briefly, 20 µL of Schiff's reagent (Cat. 1.09034 Sigma-Aldrich) were mixed with 200 µL of a suspension 1:10 of AG-Co^{2+}/A/G in distilled water. The mixture was incubated at room

temperature during 30 min with gentle mixing. Later the support was washed 4 times with 0.5 mL of 1 M NaCl followed by 5 washes of 0.5 mL of distilled water. The washed support was resuspended 1:10 in distilled water in order to measure the absorbance of 100 µL at 570 nm against a support control without GA activation (AG-IDA/A). Calibration curve of glutaraldehyde (linear range 0.15 – 2.5 mM) was also prepared under the same conditions. Micrographs of the Schiff activated AG-IDA/A were acquired by placing 100 µL of a 1:200 water suspension of the support in water in a 96-well clear bottom black microplate and visualized using a Plan Fluorite 4X phase objetive and performed color brightfield imaging, multicolored LED illumination within a Cytation5 Cell Imaging Reader (BioTek Instruments) (Supplementary, Figure S1B).

HMF groups quantitation

Agarose functionalization with HMF was spectrophotometrically quantified by a using a HMF calibration curve (linear range 0.19 mM – 1.56 mM). In order to properly determine the calibration curve, we measured the absorbance of 200 µL of a suspension (1:20) of AG-IDA/H or AG incubated with different concentrations of HMF in water at 285 nm in a Microplate Reader Epoch 2 (BioTek Instruments).

Enzyme immobilization

The immobilization was conducted by mixing 10 mL of enzyme solution (in 100 mM sodium phosphate buffer pH 7) with 1 g of support (AG-Co^{2+}/A/G or AG- Co^{2+}/A/E or AG-Co^{2+}/H). The suspension was maintained under gentle agitation at 25 rpm at 4 °C. The immobilization course was followed by measuring the activity for both the supernatant and the suspension. Once the

immobilization was completed (typically 30 minutes), the immobilization mixture was incubated for 2 h in total (including the immobilization time) at 25 rpm and 4 °C in order to promote the formation of multivalent attachment between the nucleophiles on the enzyme surface (mainly Lys) with the either the aldehydes or the epoxide of the support surface. Subsequently, a blocking step was done by addition of glycine (1 M pH 8) followed by soft agitation over night at 25 rpm and 4 ºC. Once the support was blocked, the immobilized sample was washed 5 times with 5 volumes of 25 mM sodium phosphate buffer pH 8, filtered and stored at 4 °C.

Enzyme co-immobilization

Enzyme co-immobilization was conducted following the same methodology previously described but incorporating the enzymes in two different orders. For the sequential immobilization, 10 mL of TtNOX in 100 mM sodium phosphate buffer at pH 7 were firstly incubated with 1 g of AG-Co^{2+}/A/G during 2 h at 25 rpm and 4 ºC. Afterwards, the suspension was filtered and 10 mL of a solution of BlCAT in the same buffer was added, followed by incubation for 2 h at 4 ºC and 25 rpm. Later, the suspension was filtered again and 10 mL of BsADH in the same buffer were added and incubated for 2 more hours at 4 ºC and 25 rpm. Then, the suspension was filtered and incubated overnight at 4 ºC and 25 rpm with 1 M glycine at pH 8 to block the remaining aldehyde groups. Finally, the biocatalyst was filtered ad washed with 25 mM sodium phosphate buffer pH 7 and stored at 4 ºC.

Enzyme activity assays

Enzyme activities were spectrophotometrically measured in transparent 96-well microplates with flat bottom (Nunc), employing a Microplate Reader Epoch 2 (BioTek Instruments) provided with the software Gen5.

ADH activity

200 µL of a reaction mixture containing 10 mM 1,5-pentanediol and 1 mM NAD^+ in sodium phosphate buffer at pH 8 were incubated with 5 µL of enzymatic solution or 10 µl of suspension (properly diluted) at 30 ºC. The increase in the absorbance at 340 nm due to the reduction of NAD^+ was recorded. One unit of activity was defined as the amount of enzyme that was required to reduce 1 µmol of NAD^+ to NADH per minute at the assayed conditions.

NADH oxidase activity

200 µL of a reaction mixture containing 0.2 mM NADH and 150 µM FAD^+ in 50 mM sodium phosphate buffer pH 8 at 30 ºC were incubated with 5 µL of enzymatic solution or 10 µl of suspension (properly diluted) at 30 ºC. The oxidation of NADH was monitored as a decrease in the absorbance at 340 nm. One unit of activity was defined as the amount of enzyme that was required to oxidize 1 µmol of NADH to NAD^+ per minute at the assayed conditions.

Catalase activity

200 µL of a reaction mixture containing 35 mM hydrogen peroxide in 100 mM sodium phosphate pH 8 at 30 ºC were incubated with 5 µL of the enzymatic solution or 10 µl of suspension (adequately diluted). The catalase activity was measured by recording the decrease in the

absorbance at 240 nm. One unit of CAT activity was defined as the amount of enzyme required for the disproportionation of one μmol of hydrogen peroxide per minute at the assessed conditions.

Lactonase activity

Lactonase activity was indirectly monitored by the decrease in the pH triggered by the formation of 5-hydroxypentanoic acid from its corresponding lactone hydrolysis. Briefly, 200 μL of a reaction mixture containing the 1 mM δ-valerolactone, 0.1% acetonitrile, 0.25 mM *p*-nitrophenol in 2.5 mM sodium phosphate buffer at pH 7.0 were incubated with 5 μL of enzymatic solution or 10 μl of suspension (properly diluted) at 30 ºC. The decrease in the absorbance of *p*-nitrophenol (pH indicator) at 410 nm was recorded. One unit of activity was defined as the amount of enzyme that was required to produce 1 μmol 5-hydroxypentanoic acid (titrated by pH change) per minute at the assayed conditions.

Thermal inactivation

Thermal inactivation kinetics of the biocatalysts were conducted by incubating a solution or a suspension of the free or immobilized enzymes in 100 mM sodium phosphate buffer pH 8.0 at the indicated temperature until more than 50% of the initial activity was lost. In order to calculate half-life times, the obtained experimental measurements were adjusted to a 3-parameters biexponential kinetic inactivation model.[22] Additionally, we determined the thermal denaturation temperature (Tm) of the biocatalysts by fluorescent thermal shift assay. Briefly, 25 μL of 1 μM enzyme solution of suspension in 25 mM sodium phosphate buffer pH 8 containing 5 μL 60x of SPYRO Orange Protein Gel Stain were placed into a 200 μL clear thin-wall polypropylene 8-tube strip for PCR. The protocol was set with a temperature analysis range from 25 to 95 ºC in 1 h, recording the

fluorescence in a CFX Real-Time PCR system (Bio-Rad). Raw fluorescence data were analyzed to determine the denaturation temperature (Tm) from non-linear fitting of thermal denaturation data[23] employing OriginLab software.

Protein labeling with fluorescent probes

Fluorescent labeling was done accordingly with a methodology reported elsewhere.[24] An enzyme solution (typically 0.25 $mg \cdot mL^{-1}$) in 100 mM of sodium bicarbonate buffer at pH 8.5 was mixed (1:10 molar ratio) with either rhodamine B isothiocyanate or fluorescein isothiocyanate (FITC) in DMSO (5 $mg \cdot mL^{-1}$), and incubated 1 h with gentle agitation at 25 ºC in darkness. Afterwards, the remaining fluorophore was eliminated by dialysis through centrifugal filter unit (cutoff of 10 kDa) with 25 mM sodium phosphate buffer pH 8.0.

Confocal laser scanning microscopy (CLSM) imaging

The distribution of immobilized fluorophore-labelled proteins was analyzed with a confocal microscope Espectral ZEISS LSM 510 with an excitation laser (λ_{ex}: 561 nm) and emission filter (LP575). Confocal imaging was carried out a both x20 and x40 (water, 1.2 NA) objectives and a 1:200 (w:v) buffered suspension in 25 mM phosphate at pH 7. The resulting micrographs were analyzed with FIJI[25] using an image analytical routine previously reported.[26] From confocal images, we obtained an average and normalized fluorescence radius profile, using FIJI software and its plugin module for radial profile generation (developed by Paul Baggethun). Subsequently, a Gaussian fit was applied to the obtained profiles of at least 10 single beads. Subsequently, we searched for the fitted data point that corresponds to the 50% of the maximum normalized fluorescence fitted peak (yFWHM), and the corresponding radius coordinate (xFWHM) to that

data point was then subtracted from the radius (R) of the analyzed bead to finally obtain the FWHM (full width half maximum) that means the infiltration distance of the enzyme into the bead surface. Dividing this infiltration distance between the radius size we obtained the relative infiltration distance.

Fluorescent Anisotropy

The polarized fluorescence of immobilized samples loaded with 0.5 mg of FTIC-labelled enzymes were measured to determine the fluorescence anisotropy of FTIC conjugated to the free and immobilized proteins. In order to calculate the anisotropy values, 3.5 ng of either free or immobilized enzymes were placed into a 96- well dark plate and measured in a Microplate Reader Synergy H1, BioTek®. Anisotropy values were obtained following the methodology described elsewhere.[17]

The anisotropy values of all immobilized samples were normalized to the anisotropy of the free enzyme. Values higher than one mean enzymes with higher rotational tumbling than the free enzyme, while values lower than one mean enzymes with lower rotational tumbling than the free enzyme.

Intrinsic fluorescence of tryptophans

Immobilized biocatalysts loading 0.5 mg of protein × g support $^{-1}$ were used for this experiment. The intrinsic fluorescence of free and immobilized His-BsADH was measured before and after the samples were incubated at 80°C for 1 h. To that aim, 70 μg of either free or immobilized enzymes were placed in a 96-well dark plate and the fluorescence emission spectra was recorded

between300 and 500 nm upon the sample excitation at 280 nm, using emission band widths of 5 nm. All spectroscopic measurements were performed in 25mM phosphate buffer at pH 7.

Batch reactions and recycling of co-immobilized enzymes

50 mg of heterogeneous biocatalyst were placed inside a capped plastic tube (2 mL) containing 300 µL of a reaction mixture consisted in 20 mM 1,5-pentanediol, 1 mM NAD^+, 0.15 mM FAD^+ in 100 mM sodium phosphate buffer pH 8 allowing atmospheric oxygen supplementation by punching the tap with an open needle. Reactions were incubated at 30 ºC at 250 rpm inside an orbital incubator. The reaction course was monitored by withdrawing samples at periodic intervals which were analyzed by chromatographic methods.

Chromatographic methods

Gas Chromatography (GC)

Prior to GC analysis, 50 µL of reaction sample were mixed with 200 µL of ethyl acetate to perform a liquid-liquid extraction of the compounds of interest containing 2 mM eicosane as external standard. After the extraction, 30-50 mg of anhydrous $MgSO_4$ were added to dry samples before GC analysis. Gas chromatography analyses were carried out in an Agilent 8890 GC system chromatograph using a J&W HP-5 GC column (30 m × 0.32 mm × 0.25 µm), helium as the support gas, and equipped with a flame ionization detector (FID). The injector was set at 280 ºC and the FID at 300 ºC. Separation of extracted compounds in ethyl acetate were done by the following temperature program: the initial temperature at 60 ºC, maintained 2 min, ramp to 160 ºC at a rate of 10 ºC·min^{-1}, ramp 2 to 240 ºC at a rate of 20 ºC·min-1 and finally maintained 4 min. Retention

times for 1,5-pentanediol, 5.6 min, tetrahydro-2H-pyran-2-ol, 3.4 min, δ-valerolactone, 5.8 min and eicosane (external standard) 16.4 min.

High Performance Liquid Chromatography (HPLC) analysis

5-hydroxypentanal was quantified by HPLC through derivatization into its corresponding O-benzylhydroxylamine derivative.[27] Briefly, 10 µL of aqueous reaction sample (0.6 - 20 mM) were mixed with 50 µL of O-benzylhydroxylamine hydrochloride (130 mM in pyridine/methanol/water 33:15:2) and incubated for 5 min at 25 ºC. Afterwards, 500 µL of methanol were added and then centrifuged 5 min at 13450 g. HPLC analysis was conducted in an Agilent Technologies 1260 Infinity II chromatograph equipped with a Poroshell EC-C18 column (4.6 x 100 mm, 2.7 µm). Samples were detected at 215 nm and were eluted at 1 $mL \cdot min^{-1}$ flow rate employing two mobile phases; phase A composed of trifluoroacetic acid 0.1 % in water, and phase B composed of trifluoroacetic acid 0.095% in 4:1 acetonitrile/water. Elution conditions: 10% to 100% of B over 30 min, followed by 10 min to recover the initial conditions. Retention time of O-benzylhydroxylamine derivatized 5-hydroxypentanal was 14.4 min.

Results and Discussion

Support functionalization

Ideally, an heterofunctional support should enable the efficient co-immobilization of different enzymes through chemistries that improve the overall properties of the multi-enzyme system. Inspired by a previously described tri-heterofunctional support exploited for the immobilization of single enzymes,[16] we also functionalized porous agarose microbeads with cobalt-chelates to site-directed immobilize His-tagged enzymes, with positively charged secondary amines to ionically

absorbed negatively charged enzymes and electrophile groups (aldehyde and epoxide) to react with the nucleophile residues at the enzyme surface. These three reactive groups should allow the immobilization of three different enzymes through three different chemistries (Scheme 1a).

As support, we selected 4BCL porous agarose microbeads (4 BCL with 300 nm average pore size and 90-150 μm bead diameter), which have a suitable pore diameter for the immobilization of enzymes, a suitable particle size for the use of the heterogeneous biocatalysts in both batch and flow reactors, and a great versatility to be functionalized with a plethora of reactive gorups[4]. We fist functionalized agarose microbeads with epoxy groups (AG-E), [28] and then AG-E was incubated with iminodiacetic acid (IDA) to generate the bifunctional support containing epoxy and IDA groups (AG-IDA/E) (Scheme S1). The degree of IDA functionalization is easily controlled by the pH and the incubation time (Supplementary, Table S1). After this step, we introduced a 1:1 molar ratio of epoxy:IDA groups on the modified agarose surface (19 and 20 $\mu mol \cdot g^{-1}$, respectively) (Supplementary, Table S2). Afterwards, we introduced the first target functionality, by incubating the AG-IDA/E with ethylenediamine (EDA), which converted the remaining epoxy groups into amine ones but maintaining intact the IDA ligands (AG-IDA/A). Then, the second functionality was introduced by incubating the AG-IDA/A with glutaraldehyde (G), a bifunctional agent, which reacts quantitatively with the primary amine of EDA, giving rise to a functionalized support with aldehyde and secondary amine groups (AG-IDA/A/G) (Supplementary, Scheme S1). The functionalization of AG-IDA/A with primary amines and AG-IDA/A/G with aldehydes was confirmed by titration with picrylsulfonic acid and with the Schiff reagent, respectively (Supplementary, Figure S1). Optical microcopy images reveal that the functionalization of the agarose microbeads is uniform throughout their porous structure. Finally, we incubated AG-

IDA/A/G with a cobalt chloride solution to form cobalt-chelates, which are the third functional group of the tri-functional support (AG-Co^{2+}/A/G) (Supplementary, Scheme S1). We found out that the functional groups are uniformly distributed over the porous surface of the agarose beads, enabling the enzymes to be potentially immobilized on any region (outer and inner) of the support particles. Apart from the aliphatic aldehydes, we also explored other two possible activation chemistries that functionalize the support with epoxy and aryl aldehydes (Scheme 1b). To that aim, we employed 1,4-butanediol diglycidyl ether to replace aldehyde groups of AG-Co^{2+}/A/G by epoxide ones, yielding a heterofunctional support functionalized with cobalt, amino and epoxide groups (AG-Co^{2+}/A/E, Supplementary, Scheme S2). On the other hand, we replaced GA and EDA by hydroxymethylfurfural, finally yielding an heterofunctional support functionalized with cobalt and aromatic aldehyde groups (AG-Co^{2+}/H, Supplementary, Scheme S3 and Table S2). After titration of epoxy, aldehydes, amine and cobalt chelates, the three supports were functionalized with different reactive groups in equimolar ratios per gram of support, and similar reactive group density but HMF, which its density was 3 times lower than the aldehydes and epoxy groups (Supplementary, Table S2).

Enzyme immobilization on heterofunctional supports

We selected an enzyme panel to evaluate the immobilization efficiency on the three heterofunctional supports and the stabilization effects they promote on the immobilized enzymes. Herein, the enzyme panel studied is composed of an homotretameric His-tagged alcohol dehydrogenase from *Bacillus stearothermophilus* (BsADH),[29] a dimeric alcohol dehydrogenase from horse liver (HlADH),[30] an untagged homodimeric NADH oxidase from *Thermus Thermophilus HB27*,[31, 32] an His-tagged homodimeric lactonase from *Sulfolobus islandicus*

(SiLAC),[33] an untagged tetrameric catalase from bovine liver (BlCAT)[34] and an His-tagged tetrameric catalase from *Bordetella pertussis* (BpCAT) which expresses both, higher specific activity and stability than BlCAT.[35]

All enzymes were immobilized on the three heterofunctional supports in less than two hours (Supplementary, Figure S2). Regardless the nature of the reactive groups displayed in the supports, His-tagged enzymes (as BsADH, BpCAT and SiLAC) were quantitatively immobilized, in contrast to the untagged ones (BlCAT, HlADH and NOX), which achieved slightly lower immobilization yields (> 92 %) (Table 1). With these results in hands, we demonstrate the feasibility of these heterofunctional supports to effectively immobilize a wide variety of His-tagged and untagged enzymes of different sizes and electrostatic surfaces under neutral pH conditions. These heterofunctional supports attain higher immobilization performance compared with agarose microbeads activated with cobalt-chelates and epoxy groups (AG-Co^{2+}/E), a benchmarked heterofunctional support widely used in applied biocatlaysis[36] (Supplementary, Table S3). For example, the positively amine groups displayed in the AG-Co^{2+}/A/G and AG-$Co^{2+/}$A/E surfaces seem to increase the immobilization yield up to > 90% for enzymes with few exposed lysine residues, as it is the case of TtNOX (4 exposed lysine residues, PDB 1NOX) which only reached a 54% immobilization yield on AG-Co^{2+}/E.

Table 1. Single-enzyme immobilization parameters on different heterofunctional activated agarose microbeads.

Enzyme	Immobilization support	Enzyme load ($mg \cdot g^{-1}$)	Ψ (%) [a]	Recovered activity ($U \cdot g^{-1}$) / (%) [b]	Half-life time ($t_{1/2}$) (h) [c]
BsADH	AG-Co^{2+}/A/G	0.47	100	0.42 (21)	0.51
	AG-Co^{2+}/A/E	0.47	100	0.58 (30)	0.85
	AG-Co^{2+}/H	0.47	100	0.37 (19)	0.42
HlADH	AG-Co^{2+}/A/G	1.52[d]	99	0.24 (45)	54

	AG-Co^{2+}/A/E	1.54[d]	100	0.25 (47)	21
	AG-Co^{2+}/H	1.51[d]	98	0.22 (40)	26
TtNOX	AG-Co^{2+}/A/G	1.23	92	0.76 (8.1)	9.2
	AG-Co^{2+}/A/E	1.14	94	0.14 (1.3)	15.7
	AG-Co^{2+}/H	1.16	99	0.11 (1.1)	24.0
BlCAT	AG-Co^{2+}/A/G	0.54[d]	96	12 (6.5)	4.4
	AG-Co^{2+}/A/E	0.52[d]	92	8 (4.3)	4.0
	AG-Co^{2+}/H	0.55[d]	98	11 (6.0)	3.4
BpCAT	AG-Co^{2+}/A/G	0.25	99	19 (22)	17.0
	AG-Co^{2+}/A/E	0.25	100	0 (0)	25.0
	AG-Co^{2+}/H	0.25	100	0.6 (0.7)	17.0
SiLAC	AG-Co^{2+}/A/G	0.43	100	0.18 (42)	7.4
	AG-Co^{2+}/A/E	0.43	100	0.05 (12)	4.7
	AG-Co^{2+}/H	0.43	100	0.09 (21)	6.4

[a] Immobilization yield, Ψ = (immobilized activity/offered activity) x100. [b] % Recovered activity is defined as the coefficient between the specific activity of the immobilized enzyme and the specific activity of the soluble one x 100. [c] Half-life times studies were assayed at different temperatures accordingly with each enzyme, thus 65 ºC for BsADH, 45 ºC for HLAHD, 80 ºC for TtNOX, 40 ºC for BpCAT, 45 ºC for BlCAT, and 50 ºC for SiLAC. Half-lives of the free enzymes are provided in Table S4.[d] Total protein content of semi-pure enzyme solutions.

On the other hand, we evaluated the performance of the different heterofunctional supports by comparing the recovered activity of each immobilized preparation. An ideal support would have 100% recovered activity (or immobilization effectiveness of 1), while lower values indicate enzyme inactivation upon immobilization. Immobilized enzymes follow a trend of activity reduction in all cases (Table 1). Particularly ADHs suffer 50-80% enzyme inactivation upon their quantitative immobilization on these matrixes. These results are in agreement with our previous report, where BsADH was immobilized on different epoxy-activated matrixes[17]. Unlike ADHs, the oxygen dependent NADH oxidase (TtNOX) undergoes a marked enzyme activity reduction upon immobilization (losing more than 90% of its initial activity), recovering the highest activity when using AG-Co^{2+}/A/G (8.1%). This large activity reduction effect is mainly attributed to a hampered oxygen diffusion inside the macroporous agarose structure previously reported by our

group[37]. Likewise, both catalases show marked activity reduction upon immobilization, where BlCAT retains less than 7% of its initial activity, while BpCAT expresses three-fold higher residual activity only when immobilized on AG-Co^{2+}/A/G (22%). This high activity loss, has been also reported by other authors when immobilizing BlCAT on highly glutaraldehyde-activated agarose microbeads[38]. Finally, the studied lactonase maintains 12% to 42% of its initial activity upon immobilization, where AG-Co^{2+}/A/G provides the highest recovered activity of this enzyme. Previously, we co-immobilized both, the SiLAC and BsADH on the same AG-Co^{2+} microbeads recovering 100% of its initial activity upon co-immobilization by metal-ligand affinity[39], thus we suggest that the enzyme inactivation of lactonase is triggered by the multivalent covalent attachment promoted by the GA groups.

Additionally, we assessed the thermal stability of the different heterogeneous biocatalysts at specific temperature conditions (Table 1, Supplementary, Table S4 and Fig. S3). The immobilization stabilizes the majority of the herein tested enzymes, reaching up to 20 times higher half-life times for some of them (i.e. the HlADH immobilized on AG-Co^{2+}/A/G). Surprisingly, immobilized BsADH, regardless the support, is less stable than its free counterpart. The physical and chemical congruence of BsADH and support surfaces might cause protein structural distortions that lead to a less stable biocatalyst when it is supported. This specific issue we find for BsADH may be addressed by post-immoblization polymeric coatings that stabilize the quaternary structure of oligomeric enzymes[38]. Despite the three supports efficiently immobilize all the tested enzymes with high yields, AG-Co^{2+}/A/G proves to be the optimal one to maximize the recovered activity and stability (high $t_{1/2}$ values) of a wider range of enzymes. For this reason, we select this support for further characterization studies.

Orthogonality of the immobilization chemistries in the tri-functional support AG-Co^{2+}/A/G

AG-Co^{2+}/A/G displays three different reactive groups that may immobilize enzymes through three different mechanisms to prepare immobilized multi-enzyme system with industrial relevancy. Herein, we selected three different enzymes whose immobilization requires three different chemistries; His-BsADH, TtNOX and BlCAT. In particular, TtNOX hardly interacts with cationic exchangers[32], unlike BlCAT, which strongly does with positively charged supports.[40] On the other hand, metal-chelates binds His-BsADH very efficiently and TtNOX has been successfully immobilized on supports functionalized with aldehyde as standalone reactive group.[32] Understanding the mechanism that drive the immobilization of each enzyme will allow us to design more efficiency co-immobilization protocols to fabricate highly active and stable multifunctional heterogeneous biocatalysts. The combination of these three enzymes presents a great potential in applied biocatalysis for the selective oxidation of diols into their corresponding aldehydes or lactos[17], lactones and ω-hydroxy acids[39], but also for the synthesis of aminoalcohols when coupled to transaminases[18].

To that aim, we evaluated the individual contribution of each reactive group displayed in AG-Co^{2+}/A/G to the enzyme immobilization kinetics. To study the sole contribution of cobalt-chelates, we blocked the support with glycine to remove the contribution of the aldehyde groups and performed the immobilization in presence of high salt concentration to avoid ionic interactions (sample coordination-chemistry, pink line in Figure 1). For the sole contribution of amine groups, we also blocked the aldehydes with glycine and performed the immobilization in presence of imidazole (sample ionic-chemistry, orange line in Figure 1). Finally, to study the sole contribution of the aldehydes, the immobilization was performed in presence of high concentration of salt and imidazole (sample covalent-chemistry, purple line in Figure 1). Figure 1A shows that the

immobilization of His-BsADH is driven by the cobalt-chelates groups as the immobilization rate was significantly reduced only when coordination chemistry was blocked by incubation with imidazole (purple line). For this enzyme, the aldehydes thus contribute to the first step of the immobilization to a lower extent than metal chelates. In the case of untagged TtNOX, we observe that cobalt-chelates and aldehyde groups dominate the immobilization kinetics as the enzyme is immobilized with a similar rate regardless of whether interactions with one or the other group are blocked (Figure 1B). This insight agrees with the fact that aldehyde chemistry based on agarose activated with glyoxyl groups enables an efficient immobilization of that enzyme. Likewise, it has been reported that untagged TtNOX interacts nonspecifically with metal chelates through some exposed histidine residues at its surface.[32] Finally, the immobilization of untagged BlCAT on AG-Co^{2+}/A/G is dominated by the aldehyde and amine groups, since the immobilization negligibly occur when the aldehydes were blocked and the immobilization was performed in presence of salt (Figure 1C). Blocking the interactions with the aldehydes slows down the immobilization to a similar extent as avoiding the electrostatic interactions between BlCAT and the amine groups of the support. Therefore, for the three enzymes herein studied and under this experimental set-up, AG-Co^{2+}/A/G drive the immobilization through a mixed mechanism. The type of interactions that dominate the immobilization kinetics of each enzyme therefore depends on their intrinsic physio-chemical properties. Although the specific blocking of the different reactive groups allows us understanding the mechanisms that drive the immobilization of these three model enzymes, the fastest immobilization rates were achieved when the three reactive groups of AG-Co^{2+}/A/G were available for the enzyme attachment.

In the light of this results, the aldehyde groups do not play a fundamental role for the immobilization of BsADH in the first immobilization step, however they may participate in a

slower second step where a multivalent and irreversible attachment between the enzyme and the support is promoted. The irreversibility of this immobilization was confirmed by SDS-PAGE (Supplementary, Figure S4). Enzymes are undetectably lixiviated after incubating the immobilized preparations with 0.3 M imidazole, 1 M NaCl or a combination of both. Under these conditions the enzymes only bound through cobalt-chelates and/or ionic interactions should be eluted to the bulk. However, partial enzyme lixiviation is only observed when incubating the immobilized biocatalysts at denaturing conditions (10 min boiling in β-mercaptoethanol-SDS Laemmli's lysis buffer). This fact may be related to the subunit leaching of the oligomeric enzymes due to a suboptimal geometric congruence with the support surface (Supplementary, Figure S4).

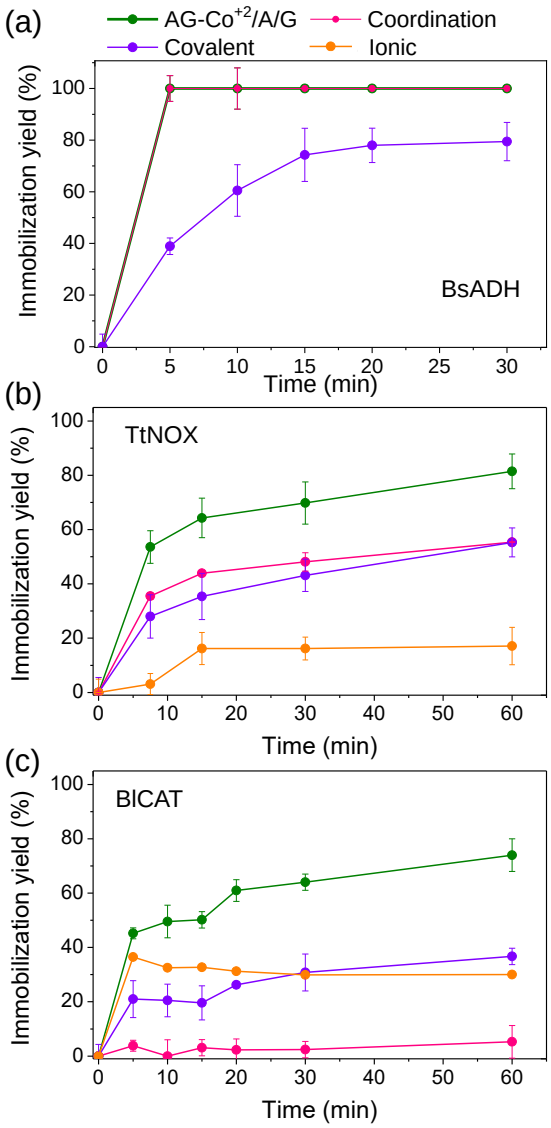

Figure 1. Driving immobilization chemistry of different enzymes (a) histidine-tagged BsADH, (b) TtNOX, and (c) BlCAT, on tri-heterofunctional activated agarose microbeads. For AG-Co^{2+}/A/G the immobilization was carried out at 100 mM sodium phosphate buffer pH 8 (green lines and symbols). To only assess the coordination chemistry (pink line), the immobilization was conducted by previously blocking G groups of AG-Co^{2+}/A/G (with glycine 1 M for 16 h) and performing the immobilization at 1 M NaCl. To only assess the covalent chemistry (purple line), the immobilization was conducted at 0.3 M imidazole and 1 M NaCl. To only assess the ionic chemistry (orange line), the immobilization was conducted by previously blocking G groups of AG-Co^{2+}/A/G (with glycine 1 M for 16 h) and performing the immobilization at 0.3 M imidazole. The green line represents the immobilization course on AG-Co^{2+}/A/G where the three chemistries can participate. In all cases, the immobilization was conducted at 4 ºC and 25 rpm.

Spatial distribution of immobilized enzymes across differently activated supports

In order to study the spatial distribution of different enzymes (BlCAT, BpCAT, BsADH, HlADH, TtNOX and SiLAC) across the inner surface of the tri-functional support, we labelled the enzymes with a fluorescent probe (Rhodamine isothiocyanate) prior their immobilization. Then, we immobilized the labelled enzymes on AG-Co^{+2}/A/G in order to investigate the enzyme distribution along the microparticle by confocal laser scanning microscopy (CLSM). From the CLSM images we calculated the relative infiltration distance defined as the percentage of radius where more than 50% of maximum fluorescence intensity of the sample is detected according to Diamanti et al.[26] His-tagged enzymes (BpCAT, BsADH and SiLAC) are located at the very outer surface of the porous agarose microbeads colonizing less than 15% of the particle radius (Figure 2). On the contrary, the untagged enzymes colonize inner regions of the beads, occupying up to the 67% of the bead radius in the case of TtNOX. The spatial organization found for the different enzymes is supported by their immobilization kinetics. As previously reported by our group,[41] high immobilization rates lead the enzymes to colonize the outer surface of porous materials since the enzyme immobilization is faster than the protein diffusion throughout the beads. On the contrary, low immobilization rates promote the enzyme infiltration toward inner regions of the beads because the protein diffusion is equal to or faster than the immobilization process. According to this, a His-tagged enzyme like BsADH only colonizes the most outer 5 μm of the bead radius (10% relative infiltration distance) thanks to its fast immobilization (100% yield in 5 minutes, Figure 1A). In contrast untagged enzymes colonize more inner regions due to their lower immobilization kinetics. For example, TtNOX is uniformly distributed across the radius of the beads because its immobilization rate is rather low (80% yield in 60 minutes, Figure 1B). This spatial organization of TtNOX explains its low recovered activity upon immobilization on this tri-functional support

as oxygen mass transport restrictions are more severe when the enzyme is located at the inner regions of porous supports. A similar insight was observed when TtNOX was uniformly distributed across aldehyde-activated agarose microbeads[37]. Regarding other untagged enzymes, we find the same trend for BlCAT (Figure 1C), yet this enzyme is infiltrated to a lower extent than TtNOX (50 KDa) likely due to its higher molecular weight (240 KDa) that may hamper its diffusion across the porous structure of the support.

(a)

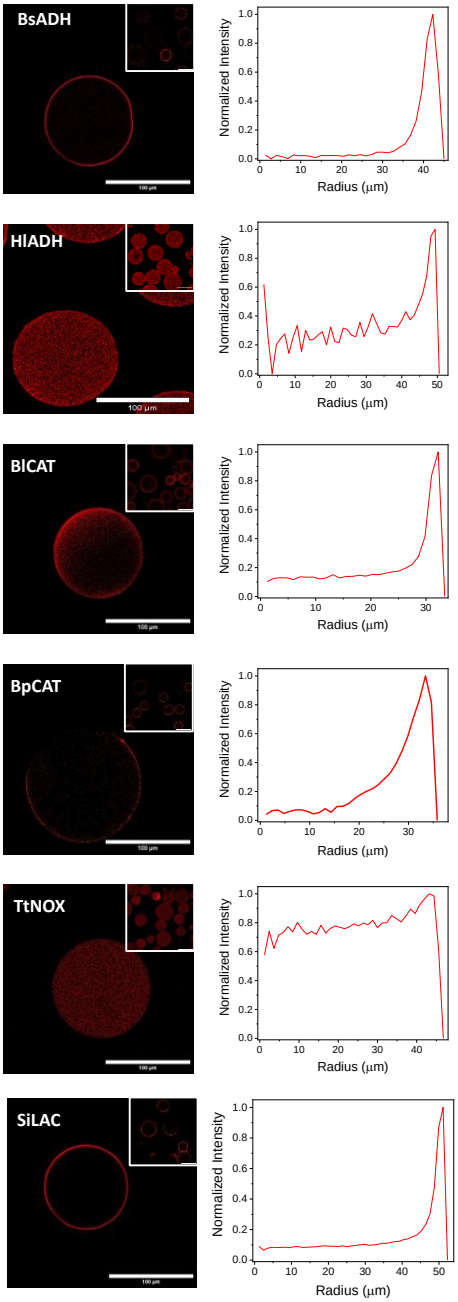
BsADH
HlADH
BlCAT
BpCAT
TtNOX
SiLAC
Normalized Intensity
Radius (μm)

(b)

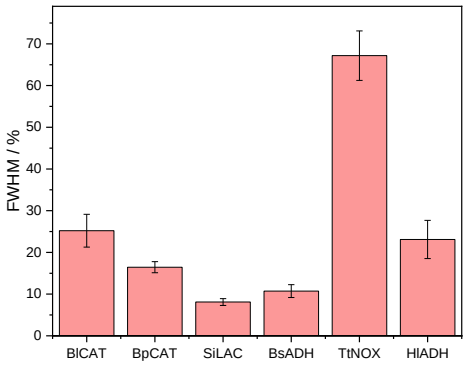
FWHM / %
BlCAT
BpCAT
SiLAC
BsADH
TtNOX
HlADH

Figure 2. (a) Confocal fluorescence microscopy of immobilized enzymes labelled with Rhodamine B (Red Chanel) and the corresponding radial profiles. (b) Infiltration penetration percentage of each immobilized enzyme across the surface of different porous supports.

Stability and structural analysis of immobilized enzymes on tri-heterofunctional supports

To better explain the effect of the immobilization on the enzyme properties, we used a set of biophysical techniques to elucidate the structural rearrangements undergone in 6 different enzymes (BsADH, HlADH, TtNOX, BlCAT, BpCAT and SiLAC) when immobilized on AG-Co^{+2}/A/G. In one hand, we studied the intrinsic fluorescence spectrum of both immobilized and free enzymes (Supplementary, Figure S5) in order to acquire information about their microenvironment within the protein structure.[42] On the other hand, we determined the relative anisotropy of free and immobilized enzymes labelled with fluorescein B isocyanate. The fluorescent anisotropy of small fluorophores tethered to the enzyme structure informs us about the apparent mobility of the protein through its rotational tumbling. The relative anisotropy of immobilized enzymes with respect to the anisotropy of their free counterpart reflects the changes in protein mobility promoted by the immobilization process. Normally, this relative anisotropy is greater as more stable the immobilized enzyme is, thus presenting a positive correlation with the half-life of the immobilized biocatalysts.[43] Finally, we determined the unfolding transition temperature (T_m) of both free and immobilized enzymes by a thermal shift assay. All these data, together with the half-life of the free and immobilized enzymes, are compiled in Table 2 for comparative purposes.

The immobilized preparation of the two ADHs, BlCAT and SiLAC presents the same λmax values than their free counterparts, indicating that the enzyme structure suffers negligible changes upon

the immobilization process. In contrast all these immobilized enzymes experience a reduction in their protein mobility (rotational tumbling) and enhancement of their Tm values and halves-lives, except BsADH which is less stable than the free enzyme although the anisotropy of the immobilized one was doubled. Specifically, immobilized TtNOX presented a red shifted λmax, which suggests that their aromatic residues are more exposed to the solvent upon the immobilization process. The more solvent accessible conformation of the immobilized TtNOX exhibits a Tm 6 ºC higher than the soluble form. This conformational change is accompanied by a reduced enzyme rotational tumbling supported by an anisotropy value almost 5 times higher than its free counterpart. Oppositely, the immobilization of BpCAT on AG-Co^{2+}/A/G results in a blue shifted λmax in comparison with its free counterpart, suggesting that its interactions with the support promote less solvent exposed aromatic residues. In this case, this interaction seems to be beneficial for BpCAT folding stability as the T_m of the immobilized enzyme is 5 ºC higher than the free one. Moreover, the higher T_m values align with the higher half-life times under thermal inactivation. In summary, almost all tested enzymes are stabilized upon their immobilization on AG-Co^{2+}/A/G reflected in their increased T_m values and half-life times, except BsADH, which shows lower thermal and folding stabilities that its free counterpart.

All assembled biocatalysts show higher anisotropy values than the free enzymes, indicating that the immobilization decreases the enzyme local mobility (rotational thumbling). Indeed, we find a trend between the anisotropy values and the thermodynamic and kinetic stability of the immobilized enzymes. T_m and half-life increase when the relative anisotropy does except for the BsADH biocatalysts. In most enzymes, the stabilization effects were accompanied by a reduction of the enzyme mobility within the porous microenvironment provided by the immobilization process and reflected in their augmented anisotropy values. In contrast, BsADH is more unstable

when its rotational mobility is limited, suggesting that less flexible conformation fixed upon its immobilization on AG-Co^{2+}/A/G is less thermally stable.

Table 2. Stabilization of immobilized enzymes on AG heterofunctional activated agarose microbeads.

Enzyme	Immobilization support	$\Delta\lambda_{max}$ (nm)	Tm (ºC)	Half-life time (h) [a]	Anisotropy
BsADH	Free	330	73	3.8	1
	AG-Co^{2+}/A/G	0	70	0.51	2.35
HlADH	Free	335	51	2.5	1
	AG-Co^{2+}/A/G	0	58	54	1.14
TtNOX	Free	335	78	3.6	1
	AG-Co^{2+}/A/G	30	84	9.2	4.62
BlCAT	Free	330	49	4.2	1
	AG-Co^{2+}/A/G	0	57	4.4	2.18
BpCAT	Free	330	56	14.5	1
	AG-Co^{2+}/A/G	-30	61	17	1.61
SiLAC	Free	335	53	3.7	1.00
	AG-Co^{2+}/A/G	0	62	6.7	2.23

[a] Half-life times studies were assayed at different temperatures accordingly with each enzyme, thus 65 ºC for BsADH, 45 ºC for HLAHD, 80 ºC for TtNOX, 40 ºC for BpCAT, 45 ºC for BlCAT, and 50 ºC for SiLAC

Co-immobilization of multi-enzyme systems

Once we characterized the separately immobilized enzymes, we assembled the multi-enzyme system formed by BsADH, TtNOX and BlCAT co-immobilizing them on the same AG-Co^{2+}/A/G microparticle. Initially, we evaluated the effect of the enzyme immobilization order on the biocatalyst activity performance. To that aim, we prepared a sequentially co-immobilized heterogeneous biocatalyst (HB1) by firstly immobilizing TtNOX, followed by the BlCAT and lastly attaching the BsADH. Likewise, we prepared a co-immobilized heterogeneous biocatalyst with the three enzymes co-immobilized at the same time (HB2) (Table 3). The immobilization

yield of TtNOX was lower when all three enzymes were co-immobilized simultaneously than when they were immobilized sequentially. This effect could be related to protein steric hindrances triggered by the fastest BsADH immobilization firstly colonizing the available matrix surface, thus exhibiting the same immobilization yields independently of the immobilization order (Table 3). The three enzyme recovered similar activities upon the immobilization regardless of whether they were immobilized sequentially (HB1) or simultaneously (HB2).

Table 3. Effect of the immobilization order on the immobilization parameters of multi-enzyme systems co-immobilized on AG-Co^{2+}/A/G.

Biocatalyst	Immobilization order	Enzymes	Enzyme load ($mg \cdot g^{-1}$)	Ψ (%) [a]	Recovered activity ($U \cdot g^{-1}$) [b] / (%) [c]
HB1	1st	TtNOX	0.78	75	1.17 (14)
	2nd	BlCAT	0.78[e]	55	598 (11)
	3rd	BsADH	0.36	100	1.25 (42)
HB2	At the same time	TtNOX	0.53	51	0.93 (16)
		BlCAT	0.80[d]	57	696 (11)
		BsADH	0.36	100	1.23 (41)

[a] Immobilization yield, Ψ = (immobilized activity/offered activity) x100. [b] Recovered activity of the immobilized enzyme per gram of support after the immobilization process. [c] (%) is defined as the coefficient between the specific activity of the immobilized enzymes and the specific activity of the soluble ones. [d] Total protein content.

Afterwards, we evaluated both biocatalysts HB1 and HB2 under operational conditions by performing a model biotransformation. For that purpose, we applied HB1 and HB2 to selectively oxidize of 1,5-pentanediol to its corresponding products (5-hydroxypentanal, tetrahydro-2H-pyran-2-ol, δ-valerolactone) in batch operation conditions according to the enzyme selectivity previously reported by our group.[17] We selected this model biocascade since allows us evaluating the coupling efficiency of the three enzymes to simultaneously oxidizing the substrate, recycling a cofactor; the NAD^+, and removing a toxic by-product; the H_2O_2 (Figure 3A). After 24 hours, both heterogeneous biocatalysts consumed more than 70% of the initial substrate 1,5-pentanediol,

yielding a similar product profile, where tetrahydro-2H-pyran-2-ol was the major product (around 60%) (Figures 3B and 3C). In agreement with the recovered activity (Table 3), the performance of the multi-enzyme system was negligibly affected by the co-immobilization order. However, after 5 hours the reactions reach a plateau for the consumption of the diol, suggesting the partial inactivation of the BsADH.

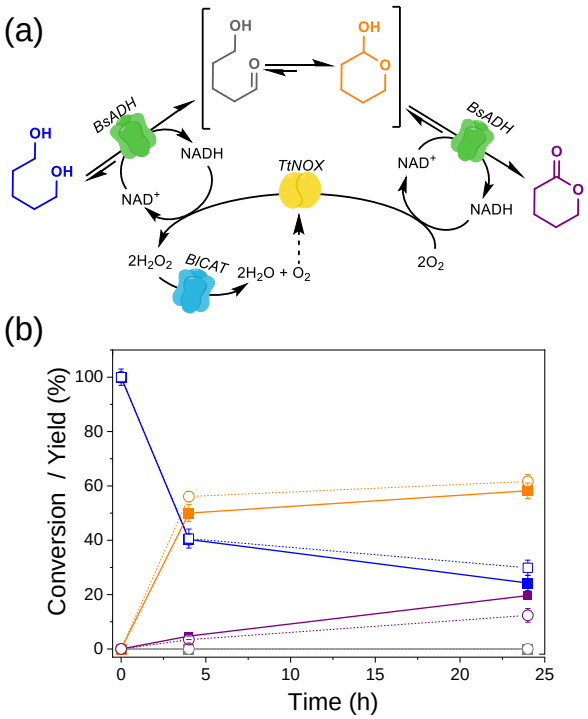

Figure 3. (a) Reaction scheme of the selective oxidation of 1,5-pentanodiol integrating NAD^+ recycling and H_2O_2 removal systems. Time courses of the 1,5-pentanodiol oxidation catalyzed by tri-enzyme systems co-immobilized on AG-Co^{2+}/A/G either sequentially (solid lines and full squares) or simultaneously (dashed lines and empty circles). 1,5-pentanediol (blue line), 5-hydroxypentanal (gray line), tetrahydro-2H-pyran-2-ol (orange line) and δ-valerolactone (magenta line). In all cases reactions were performed by incubating 50 mg of heterogeneous biocatalysts with 300 µL of reaction mixture composed by 20 mM 1,5-pentanediol, 1 mM NAD^+, 0.15 mM FAD^+ in 100 mM sodium phosphate buffer pH 8 at 30 ºC.

A spectrophotometric assay confirmed that BsADH is dramatically inactivated upon 8 h of operational use maintaining only 20% of its initial activity after 24 h (Supplementary, Figure S6). Despite this inactivation issue, the co-immobilized multi-enzyme system (HB2) reaches a 18% higher substrate consumption after 24 h than their soluble counterpart enzymes, supporting the fact that catalytic efficiency increases when multi-enzyme system is immobilized within the same confined space (Supplementary, Figure S7).

Expanding the functionalization chemistry to other materials

Apart from agarose microbeads, we expanded the developed functionalization chemistry to other typically employed materials for enzyme immobilization. To this aim, we functionalized commercially available methacrylate microbeads and macroporous cellulose beads with the same active groups than AG-Co^{2+}/A/G (referred as Pu-Co^{2+}/A/G and CE-Co^{2+}/A/G, respectively). Then, we simultaneously co-immobilized BsADH, TtNOX and BlCAT on these two other materials to evaluate their performance (Table 4). BsADH achieves similar immobilization yield on AG-Co^{2+}/A/G and Pu-Co^{2+}/A/G, but slightly lower on CE-Co^{2+}/A/G. However, the cellulose-based carrier promoted a dramatic inactivation of this enzyme upon the immobilizaiton. TtNOX behaves very similar when co-immobilized on hydrophilic matrixes as AG-Co^{2+}/A/G and CE-Co^{2+}/A/G. In contrast, this enzyme achieves higher immobilization yields when immobilized on Pu-Co^{2+}/A/G but recovers 2.4-times lower activity upon its immobilization on this hydrophobic support. According to our previous results, [37] the hydrophobicity of the support surfaces favors the immobilization of TtNOX at the expense of enzyme inactivation. Finally, BlCAT attains different immobilization yields depending on the matrix composition but expressing two times higher specific activity on agarose based supports than on cellulose and metracrylate ones. In summary, all enzymes recovered the highest activities upon the immobilization on the most hydrophilic

support (agarose microbeads) herein tested. Therefore, the physicochemical properties of the support directly affect the performance of the immobilized enzymes, even though they are immobilized through the same chemistry.

Table 4. Co-immobilization of multi-enzyme systems on tri-hetero-activated supports.

Biocatalyst	Support	Enzymes	Enzyme load ($mg \cdot g^{-1}$)	Ψ (%) [a]	Recovered Activity ($U \cdot g^{-1}$)/ (%) [b]
HB2-AG	AG-Co^{2+}/A/G	TtNOX	0.53	51	0.93 (16)
		BlCAT	0.80[c]	57	626 (11)
		BsADH	0.36	100	1.23 (41)
HB2-Pu	Pu-Co^{2+}/A/G	TtNOX	0.68	97	0.95 (6.6)
		BlCAT	0.75[c]	74	254 (5)
		BsADH	0.30	100	0.84 (28)
HB2-CE	CE-Co^{2+}/A/G	TtNOX	0.35	50	1.1 (15)
		BlCAT	0.36[c]	35	107 (4)
		BsADH	0.30	73	0.068 (3)

[a] Immobilization yield, Ψ = (immobilized activity/offered activity) x100. [b] Recovered activity of the immobilized enzyme (%) is defined as the coefficient between the specific activity of the immobilized enzymes and the specific activity of the soluble ones. [c] Total protein content

Biocatalyst recycling

As the last part of our study, we compared the reusability performance of HB2-AG, HB2-Pu and HB2-CE during the oxidation of the same model substrate in repeated batch cycles (Figure 4). The agarose-based biocatalyst (HB2-AG) shows the higher yield and operational stability among the supports studied. The first cycle conversion of 1,5-pentanodiol was 1.3 and 2.8 times larger when immobilized the multi-enzyme system on AG-Co^{2+}/A/G than on Pu-Co^{2+}/A/G and CE-Co^{2+}/A/G, respectively. Remarkably, the system immobilized on agarose microbeads maintain more than 80% of its initial activity after the second batch reaction cycle. Hence, this multi-functional heterogeneous biocatalyst is stable for more than 48 h of discontinuous operation as each reaction

cycle corresponds to 24 h of reaction at pH 8 and 30 ºC. In the three support herein analyzed, the decrease of the product yield along the cycles is supported by the dramatic inactivation found for the co-immobilized BsADH and BlCAT after the 5th batch cycle (Supplementary, Table S5). However, the further stabilization of these enzyme under these operational conditions is out of the scope of this work. Previously, BsADH was thermostabilized by its immobilization on agarose supports functionalized with epoxy and cobalt chelates, noteworthy the BsADH thermostabilization did not afford enhanced operational stability.[17] The highest operational stabilization achieved when the multi-enzyme system is immobilized on AG-Co^{2+}/A/G leads to an accumulated total turnover number (TTN, defined as the mol of oxidized 1,5-pentanediol and tetrahydro-2H-pyran-2-ol per mol of tetrameric BsADH) of 1 x 10^4 after 5 batch cycles (Figure 4b). This TTN is 325% higher than the same multi-enzyme system immobilized on CE-Co^{2+}/A/G, respectively. Expectedly, the accumulated TTN reaches a plateau upon the 4th cycle due to the inactivation of the enzymes. To note, the lower turnover of the multi-enzyme system immobilized on the cellulose-based support is attributed to the low recovered activity of BsADH upon its immobilization on CE-Co^{2+}/A/G, respectively (Table 4).

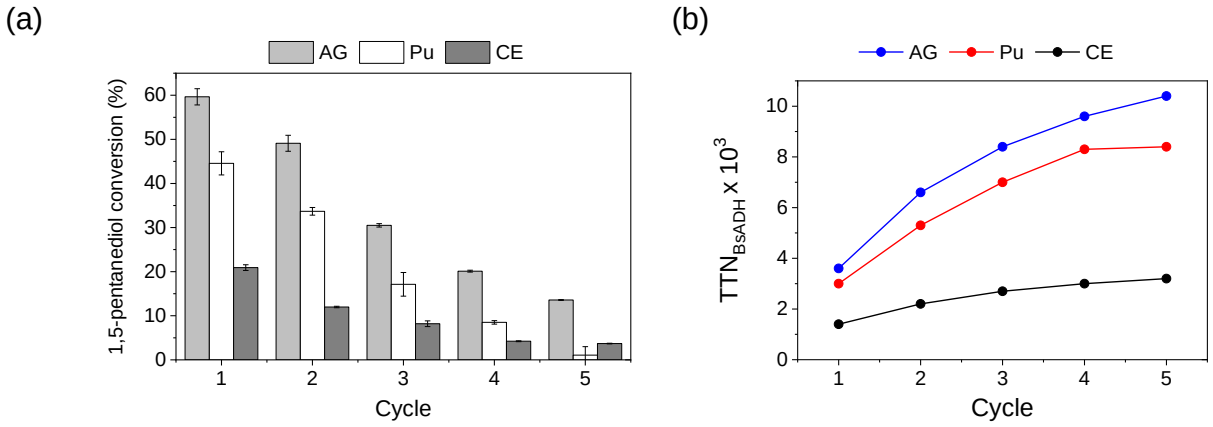

Figure 4. Recycling of co-immobilized heterogeneous biocatalysts during the oxidation of 1,5-pentanediol. A) Each cycle corresponds to 24 h working at 20 mM 1,5-pentanediol, 1 mM NAD^+, 0.15 mM FAD^+ in 100 mM sodium phosphate buffer pH 8 at 30 ºC. B) Accumulated TTN of

BsADH during recycling, defined as the mol of oxidized 1,5-pentanediol and tetrahydro-2H-pyran-2-ol per mol of tetrameric BsADH after the fifth cycle.

Conclusions

We describe the preparation of an heterofunctional support that enables the co-immobilization of a variety of enzymes requiring different immobilization chemistries. The herein characterized support possesses three chemical functionalities, namely amino, aldehyde and cobalt moieties which synergistically permit a fast irreversible enzyme immobilization at neutral pH values of His-tagged and untagged enzymes. Moreover, it is also possible to change the chemical nature of the aldehyde moiety by replacing it by an epoxide or aromatic aldehyde such as hydroxymethylfurfural. We found that aldehyde groups as electrophiles to establish covalent bonds between the enzymes and the support outperform the other two. With this information in hand, we exploited this tri-functional carrier to co-immobilize a tri-enzyme systems for the regioselective oxidation of 1,5-pentanodiol to its corresponding lactol and lactone derivatives. Additionally, we also showed the possibility to expand this surface chemistry to different porous materials such as cellulose and methacrylate microbeads, however the physicochemical properties of the support surface impact on the operational performance and stability of the co-immobilized systems. Thus, this tri-functional support demonstrates its versatility to co-immobilize a wide variety of different enzymes under mild immobilization conditions, opening the possibility to co-immobilize multi-enzyme systems aimed at enhancing the efficiency of cascade biotransformations.

ASSOCIATED CONTENT

Supplementary Content available. Supplementary schemes including the preparation of AG-Co^{2+}/A/G, AG-Co^{2+}/A/E and AG-Co^{2+}/H. Supplementary figures including the distribution of agarose-activated microbeads with different functionalities, immobilization and thermal inactivation kinetics, enzyme desorption assays, spectra of intrinsic protein fluorescence, residual activity of HBs under operation conditions and consumed 1,5-pentanediol after 24 h by the soluble or co-immobilized enzymes. Supplementary tables including activation degree of agarose-microbeads, immobilization parameters on AG-Co^{2+}/E microbeads, thermal stability of soluble enzymes and individual residual activity of co-immobilized enzymes after five batch cycles.

AUTHOR INFORMATION

Corresponding Authors

F. López-Gallego, phone +34 943003500 Ext 309, e-mail address flopez@cicbiomagune.es

S. Velasco-Lozano, phone +34 976762271, e-mail address svelasco@unizar.es

Author Contributions

FJS and SV carried out the experimental work, data analysis and curation. FLG and SV conceptualized the work. FLG supervised, managed the project administration and funding acquisition. The manuscript was written through contributions of all authors. All authors have given approval to the final version of the manuscript.

Funding Sources

This work has been funded by Era-CoBiotech (Project ID: 61 HOMBIOCAT), ERC-CoG-2018 (Project ID: 818089 METACELL), and Spanish State Research Agency (AIE) (RTI 2018-094398-B-I00, PCI 2018-092984). This work was performed under the Maria de Maeztu Units of Excellence Program from the Spanish State Research Agency—Grant no. MDM-2017-0720 (CIC biomaGUNE).

ACKNOWLEDGMENT

We acknowledge Purolite STL for kindly donating the methacrylate-based supports used in this study.

ABBREVIATIONS

ADH, alcohol dehydrogenase; BsADH, alcohol dehydrogenase from *Bacillus stearothermophilus*; HlADH, alcohol dehydrogenase from horse liver; TtNOX, NADH oxidase from *Thermus thermophilus*; BlCAT, catalase from bovine liver; BpCAT, catalase from *Bordetella pertussis*; SiLAC, lactonase from *Sulfolobus islandicus*; HB, heterogeneous biocatalyst; E, epoxy goups; EDA, ethylenediamine; IDA, iminodiacetic acid; GA, glutaraldehyde; BD, 1,4-butanediol diglycidyl ether; HMF, hydroxymethylfurfural; A, amine groups; G, aldehyde groups; H, hydrophobic aldehyde groups; AG-E, epoxy activated AG; AG-IDA/E, AG functionalized with epoxide and IDA groups; AG-$Co^{2+/}$A/G, AG functionalized with GA, EDA and IDA/cobalt groups; AG-$Co^{2+/}$A/E, AG functionalized with BD epoxide, EDA and IDA/cobalt groups; AG-$Co^{2+/}$H, AG functionalized with HMF and IDA/cobalt groups; AG, 4% cross-linked agarose beads; Pu, epoxy methacrylate microbeads ECR8204F; CE, cellulose MT200 microbeads; NAD^+,

Nicotinamide adenine dinucleotide; NADH, Reduced nicotinamide adenine dinucleotide; FAD^+, Flavin adenine dinucleotide; K_M, Michaelis-Menten constant; TTN, Total turnover number.

REFERENCES

(1) Singh, R. K.; Tiwari, M. K.; Singh, R.; Lee, J.-K. From Protein Engineering to Immobilization: Promising Strategies for the Upgrade of Industrial Enzymes. *International Journal of Molecular Sciences* **2013**, *14* (1), 1232-1277. Cipolatti, E. P.; Silva, M. J. A.; Klein, M.; Feddern, V.; Feltes, M. M. C.; Oliveira, J. V.; Ninow, J. L.; de Oliveira, D. Current status and trends in enzymatic nanoimmobilization. *Journal of Molecular Catalysis B: Enzymatic* **2014**, *99*, 56-67. DOI: https://doi.org/10.1016/j.molcatb.2013.10.019. DiCosimo, R.; McAuliffe, J.; Poulose, A. J.; Bohlmann, G. Industrial use of immobilized enzymes. *Chemical Society Reviews* **2013**, *42* (15), 6437-6474, 10.1039/C3CS35506C. DOI: 10.1039/C3CS35506C. Benítez-Mateos, A. I.; Roura Padrosa, D.; Paradisi, F. Multistep enzyme cascades as a route towards green and sustainable pharmaceutical syntheses. *Nature Chemistry* **2022**, *14* (5), 489-499. DOI: 10.1038/s41557-022-00931-2.

(2) Guisan, J. M.; López-Gallego, F.; Bolivar, J. M.; Rocha-Martín, J.; Fernandez-Lorente, G. The Science of Enzyme Immobilization. In *Methods in Molecular Biology*, 2020; Vol. 2100, pp 1-26.

(3) Stepankova, V.; Bidmanova, S.; Koudelakova, T.; Prokop, Z.; Chaloupkova, R.; Damborsky, J. Strategies for Stabilization of Enzymes in Organic Solvents. *ACS Catal.* **2013**, *3* (12), 2823-2836. DOI: 10.1021/cs400684x. Bommarius, A. S.; Paye, M. F. Stabilizing biocatalysts. *Chemical Society Reviews* **2013**, *42* (15), 6534-6565, Article. DOI: http://doi.org/10.1039/c3cs60137d Scopus.

(4) Montoya, N. A.; Roth, R. E.; Funk, E. K.; Gao, P.; Corbin, D. R.; Shiflett, M. B. Review on porous materials for the thermal stabilization of proteins. *Microporous and Mesoporous Materials* **2022**, *333*, 111750. DOI: https://doi.org/10.1016/j.micromeso.2022.111750.

(5) Rodrigues, R. C.; Berenguer-Murcia, Á.; Carballares, D.; Morellon-Sterling, R.; Fernandez-Lafuente, R. Stabilization of enzymes via immobilization: Multipoint covalent attachment and other stabilization strategies. *Biotechnology Advances* **2021**, *52*, 107821. DOI: https://doi.org/10.1016/j.biotechadv.2021.107821.

(6) Mateo, C.; Palomo, J. M.; Fernandez-Lorente, G.; Guisan, J. M.; Fernandez-Lafuente, R. Improvement of enzyme activity, stability and selectivity via immobilization techniques. *Enzyme Microb. Technol.* **2007**, *40* (6), 1451-1463, Review. DOI: http://doi.org/10.1016/j.enzmictec.2007.01.018 Scopus. Palomo, J. M. Modulation of enzymes selectivity via immobilization. *Current Organic Synthesis* **2009**, *6* (1), 1-14, Review. DOI: http://doi.org/10.2174/157017909787314885 Scopus. Rodrigues, R. C.; Ortiz, C.; Berenguer-Murcia, Á.; Torres, R.; Fernández-Lafuente, R. Modifying enzyme activity and selectivity by immobilization. *Chemical Society Reviews* **2013**, *42* (15), 6290-6307, 10.1039/C2CS35231A. DOI: 10.1039/C2CS35231A. Velasco-Lozano, S.; López-Gallego, F.; Juan C. Mateos-Díaz, J. C.; Favela-Torres, E. Cross-linked enzyme aggregates (CLEA) in enzyme improvement – a review. *Biocatalysis* **2016**, (1), 166. DOI: https://doi.org/10.1515/boca-2015-0012.

(7) López-Gallego, F.; Jackson, E.; Betancor, L. Heterogeneous Systems Biocatalysis: The Path to the Fabrication of Self-Sufficient Artificial Metabolic Cells. *Chemistry – A European Journal* **2017**, *23* (71), 17841-17849. DOI: 10.1002/chem.201703593. Velasco-Lozano, S.; López-Gallego, F. Wiring step-wise reactions with immobilized multi-enzyme systems. *Biocatal. Biotransformation* **2018**, *36* (3), 184-194, Review. DOI: 10.1080/10242422.2017.1310208 Scopus. Hartley, C. J.; Williams, C. C.; Scoble, J. A.; Churches, Q. I.; North, A.; French, N. G.; Nebl, T.; Coia, G.; Warden, A. C.; Simpson, G.; et al. Engineered enzymes that retain and regenerate their cofactors enable continuous-flow biocatalysis. *Nature Catalysis* **2019**, *2* (11), 1006-1015. DOI: 10.1038/s41929-019-0353-0. Schmidt-Dannert, C.; Lopez-Gallego, F. A roadmap for biocatalysis – functional and spatial orchestration of enzyme cascades. *Microbial Biotechnology* **2016**, *9* (5), 601-609. DOI: https://doi.org/10.1111/1751-7915.12386.

(8) Jiang, C.; Cheng, G.; Xu, F.; Wu, Q. One pot enzyme-catalyzed cascade benefit systems. *Mini-Reviews in Organic Chemistry* **2021**, *18* (3), 282-295. DOI: 10.2174/1570193X17999200727203215.

(9) Schrittwieser, J. H.; Velikogne, S.; Hall, M.; Kroutil, W. Artificial Biocatalytic Linear Cascades for Preparation of Organic Molecules. *Chemical Reviews* **2018**, *118* (1), 270-348. DOI: http://doi.org/10.1021/acs.chemrev.7b00033.

(10) Wheeldon, I.; Minteer, S. D.; Banta, S.; Barton, S. C.; Atanassov, P.; Sigman, M. Substrate channelling as an approach to cascade reactions. *Nature Chemistry* **2016**, *8* (4), 299-309. DOI: 10.1038/nchem.2459. Schoffelen, S.; van Hest, J. C. M. Chemical approaches for the construction

of multi-enzyme reaction systems. *Current Opinion in Structural Biology* **2013**, *23* (4), 613-621. DOI: https://doi.org/10.1016/j.sbi.2013.06.010. Quin, M. B.; Wallin, K. K.; Zhang, G.; Schmidt-Dannert, C. Spatial organization of multi-enzyme biocatalytic cascades. *Organic & Biomolecular Chemistry* **2017**, *15* (20), 4260-4271, 10.1039/C7OB00391A. DOI: 10.1039/C7OB00391A.

(11) Arana-Peña, S.; Carballares, D.; Morellon-Sterlling, R.; Berenguer-Murcia, Á.; Alcántara, A. R.; Rodrigues, R. C.; Fernandez-Lafuente, R. Enzyme co-immobilization: Always the biocatalyst designers' choice…or not? *Biotechnology Advances* **2021**, *51*, 107584. DOI: https://doi.org/10.1016/j.biotechadv.2020.107584.

(12) Trobo-Maseda, L.; Orrego, A. H.; Romero-Fernández, M.; Guisan, J. M.; Rocha-Martín, J. Immobilization of Enzymes on Hetero-Functional Supports: Physical Adsorption Plus Additional Covalent Immobilization. In *Methods in Molecular Biology*, Vol. 2100; 2020; pp 159-174. Zaak, H.; Sassi, M.; Fernandez-Lafuente, R. A new heterofunctional amino-vinyl sulfone support to immobilize enzymes: Application to the stabilization of β-galactosidase from Aspergillus oryzae. *Process Biochemistry* **2018**, *64*, 200-205. DOI: https://doi.org/10.1016/j.procbio.2017.09.020.

(13) Mateo, C.; Bolivar, J. M.; Godoy, C. A.; Rocha-Martin, J.; Pessela, B. C.; Curiel, J. A.; Muñoz, R.; Guisan, J. M.; Fernández-Lorente, G. Improvement of Enzyme Properties with a Two-Step Immobilizaton Process on Novel Heterofunctional Supports. *Biomacromolecules* **2010**, *11* (11), 3112-3117. DOI: 10.1021/bm100916r.

(14) Barbosa, O.; Torres, R.; Ortiz, C.; Berenguer-Murcia, Á.; Rodrigues, R. C.; Fernandez-Lafuente, R. Heterofunctional Supports in Enzyme Immobilization: From Traditional Immobilization Protocols to Opportunities in Tuning Enzyme Properties. *Biomacromolecules* **2013**, *14* (8), 2433-2462. DOI: 10.1021/bm400762h.

(15) Rocha-Martín, J.; Rivas, B. d. l.; Muñoz, R.; Guisán, J. M.; López-Gallego, F. Rational Co-Immobilization of Bi-Enzyme Cascades on Porous Supports and their Applications in Bio-Redox Reactions with In Situ Recycling of Soluble Cofactors. *ChemCatChem* **2012**, *4* (9), 1279-1288. DOI: https://doi.org/10.1002/cctc.201200146. Bié, J.; Sepodes, B.; Fernandes, P. C. B.; Ribeiro, M. H. L. Enzyme Immobilization and Co-Immobilization: Main Framework, Advances and Some Applications. *Processes* **2022**, *10* (3), 494. Velasco-Lozano, S.; da Silva, E. S.; Llop, J.; López-Gallego, F. Sustainable and Continuous Synthesis of Enantiopure l-Amino Acids by Using a Versatile Immobilised Multienzyme System. *ChemBioChem* **2018**, *19* (4), 395-403, Article. DOI: 10.1002/cbic.201700493 Scopus.

(16) Melo, R. R. d.; Alnoch, R. C.; Vilela, A. F. L.; Souza, E. M. d.; Krieger, N.; Ruller, R.; Sato, H. H.; Mateo, C. New Heterofunctional Supports Based on Glutaraldehyde-Activation: A Tool for Enzyme Immobilization at Neutral pH. *Molecules* **2017**, *22* (7), 1088.

(17) Santiago-Arcos, J.; Velasco-Lozano, S.; Diamanti, E.; Cortajarena, A. L.; López-Gallego, F. Immobilization Screening and Characterization of an Alcohol Dehydrogenase and its Application to the Multi-Enzymatic Selective Oxidation of 1,-Omega-Diols. *Front. Chem.* **2021**, *1* (9), Original Research. DOI: 10.3389/fctls.2021.715075.

(18) Velasco-Lozano, S.; Santiago-Arcos, J.; Mayoral, J. A.; López-Gallego, F. Co-immobilization and Colocalization of Multi-Enzyme Systems for the Cell-Free Biosynthesis of Aminoalcohols. *ChemCatChem* **2020**, *12* (11), 3030-3041. DOI: http://doi.org/10.1002/cctc.201902404.

(19) Guisán, J. Aldehyde-agarose gels as activated supports for immobilization-stabilization of enzymes. *Enzyme Microb. Technol.* **1988**, *10* (6), 375-382. DOI: https://doi.org/10.1016/0141-0229(88)90018-X.

(20) Snyder, S. L.; Sobocinski, P. Z. An improved 2,4,6-trinitrobenzenesulfonic acid method for the determination of amines. *Analytical Biochemistry* **1975**, *64* (1), 284-288. DOI: https://doi.org/10.1016/0003-2697(75)90431-5.

(21) Miksch, R. R.; Anthon, D. W.; Fanning, L. Z.; Hollowell, C. D.; Revzan, K.; Glanville, J. Modified pararosaniline method for the determination of formaldehyde in air. *Analytical Chemistry* **1981**, *53* (13), 2118-2123. DOI: 10.1021/ac00236a040.

(22) Aymard, C.; Belarbi, A. Kinetics of thermal deactivation of enzymes: a simple three parameters phenomenological model can describe the decay of enzyme activity, irrespectively of the mechanism. *Enzyme Microb. Technol.* **2000**, *27* (8), 612-618. DOI: http://doi.org/10.1016/s0141-0229(00)00258-1 PubMed.

(23) Huynh, K.; Partch, C. L. Analysis of Protein Stability and Ligand Interactions by Thermal Shift Assay. *Current Protocols in Protein Science* **2015**, *79* (1), 28.29.21-28.29.14. DOI: https://doi.org/10.1002/0471140864.ps2809s79.

(24) Holmes, K. L.; Lantz, L. M. Chapter 9 Protein labeling with fluorescent probes. In *Methods in Cell Biology*, Vol. 63; Academic Press, 2001; pp 185-204.

(25) Schindelin, J.; Arganda-Carreras, I.; Frise, E.; Kaynig, V.; Longair, M.; Pietzsch, T.; Preibisch, S.; Rueden, C.; Saalfeld, S.; Schmid, B.; et al. Fiji: an open-source platform for biological-image analysis. *Nature Methods* **2012**, *9* (7), 676-682. DOI: 10.1038/nmeth.2019.

(26) Diamanti, E.; Arana-Peña, S.; Ramos-Cabrer, P.; Comino, N.; Carballares, D.; Fernandez-Lafuente, R.; López-Gallego, F. Intraparticle Macromolecular Migration Alters the Structure and Function of Proteins Reversibly Immobilized on Porous Microbeads. *Advanced Materials Interfaces* **2022**, *9* (18), 2200263. DOI: https://doi.org/10.1002/admi.202200263.

(27) Hernandez, K.; Bujons, J.; Joglar, J.; Charnock, S. J.; Domínguez de María, P.; Fessner, W. D.; Clapés, P. Combining Aldolases and Transaminases for the Synthesis of 2-Amino-4-hydroxybutanoic Acid. *ACS Catal.* **2017**, *7* (3), 1707-1711. DOI: 10.1021/acscatal.6b03181.

(28) Mateo, C.; Abian, O.; Fernandez–Lafuente, R.; Guisan, J. M. Increase in conformational stability of enzymes immobilized on epoxy-activated supports by favoring additional multipoint covalent attachment☆. *Enzyme Microb. Technol.* **2000**, *26* (7), 509-515. DOI: https://doi.org/10.1016/S0141-0229(99)00188-X.

(29) Guagliardi, A.; Martino, M.; Iaccarino, I.; Rosa, M. D.; Rossi, M.; Bartolucci, S. Purification and characterization of the alcohol dehydrogenase from a novel strain of Bacillus stearothermophilus growing at 70°C. *The International Journal of Biochemistry & Cell Biology* **1996**, *28* (2), 239-246. DOI: https://doi.org/10.1016/1357-2725(95)00138-7.

(30) Ramaswamy, S.; Eklund, H.; Plapp, B. V. Structures of Horse Liver Alcohol Dehydrogenase Complexed with NAD+ and Substituted Benzyl Alcohols. *Biochem.* **1994**, *33* (17), 5230-5237. DOI: 10.1021/bi00183a028.

(31) Hecht, H. J.; Erdmann, H.; Park, H. J.; Sprinzl, M.; Schmid, R. D. Crystal structure of NADH oxidase from Thermus thermophilus. *Nature Structural Biology* **1995**, *2* (12), 1109-1114. DOI: 10.1038/nsb1295-1109.

(32) Rocha-Martín, J.; Vega, D.; Bolivar, J. M.; Godoy, C. A.; Hidalgo, A.; Berenguer, J.; Guisán, J. M.; López-Gallego, F. New biotechnological perspectives of a NADH oxidase variant from Thermus thermophilus HB27 as NAD+-recycling enzyme. *BMC Biotechnol.* **2011**, *11* (1), 101. DOI: 10.1186/1472-6750-11-101.

(33) Hiblot, J.; Gotthard, G.; Chabriere, E.; Elias, M. Structural and Enzymatic characterization of the lactonase SisLac from Sulfolobus islandicus. *PLOS ONE* **2012**, *7* (10), e47028. DOI: 10.1371/journal.pone.0047028.

(34) Nannenga, B. L.; Shi, D.; Hattne, J.; Reyes, F. E.; Gonen, T. Structure of catalase determined by MicroED. *eLife* **2014**, *3*, e03600. DOI: 10.7554/eLife.03600.

(35) Switala, J.; Loewen, P. C. Diversity of properties among catalases. *Archives of Biochemistry and Biophysics* **2002**, *401* (2), 145-154. DOI: https://doi.org/10.1016/S0003-9861(02)00049-8.

(36) Romero-Fernández, M.; Paradisi, F. Protein immobilization technology for flow biocatalysis. *Current Opinion in Chemical Biology* **2020**, *55*, 1-8. DOI: https://doi.org/10.1016/j.cbpa.2019.11.008.

(37) Benítez-Mateos, A. I.; Huber, C.; Nidetzky, B.; Bolivar, J. M.; López-Gallego, F. Design of the Enzyme–Carrier Interface to Overcome the O2 and NADH Mass Transfer Limitations of an Immobilized Flavin Oxidase. *ACS Appl. Mater. Interfaces* **2020**, *12* (50), 56027-56038. DOI: 10.1021/acsami.0c17568.

(38) Betancor, L.; Hidalgo, A.; Fernández-Lorente, G.; Mateo, C.; Fernández-Lafuente, R.; Guisan, J. M. Preparation of a Stable Biocatalyst of Bovine Liver Catalase Using Immobilization and Postimmobilization Techniques. *Biotechnol. Prog.* **2003**, *19* (3), 763-767. DOI: https://doi.org/10.1021/bp025785m.

(39) Velasco-Lozano, S.; Santiago-Arcos, J.; Grazia Rubanu, M.; López-Gallego, F. Cell-Free Biosynthesis of ω-Hydroxy Acids Boosted by a Synergistic Combination of Alcohol Dehydrogenases. *ChemSusChem* **2022**, *n/a* (n/a), e202200397. DOI: https://doi.org/10.1002/cssc.202200397.

(40) Pessela, B. C. C.; Munilla, R.; Betancor, L.; Fuentes, M.; Carrascosa, A. V.; Vian, A.; Fernandez-Lafuente, R.; Guisán, J. M. Ion exchange using poorly activated supports, an easy way for purification of large proteins. *Journal of Chromatography A* **2004**, *1034* (1), 155-159. DOI: https://doi.org/10.1016/j.chroma.2004.01.061.

(41) Bolivar, J. M.; Hidalgo, A.; Sánchez-Ruiloba, L.; Berenguer, J.; Guisán, J. M.; López-Gallego, F. Modulation of the distribution of small proteins within porous matrixes by smart-control of the immobilization rate. *J. Biotechnol.* **2011**, *155* (4), 412-420. DOI: https://doi.org/10.1016/j.jbiotec.2011.07.039.

(42) Royer, C. A. Probing Protein Folding and Conformational Transitions with Fluorescence. *Chemical Reviews* **2006**, *106* (5), 1769-1784. DOI: 10.1021/cr0404390.

(43) Orrego, A. H.; García, C.; Mancheño, J. M.; Guisán, J. M.; Lillo, M. P.; López-Gallego, F. Two-Photon Fluorescence Anisotropy Imaging to Elucidate the Dynamics and the Stability of

Immobilized Proteins. *The Journal of Physical Chemistry B* **2016**, *120* (3), 485-491. DOI: 10.1021/acs.jpcb.5b12385. García-Marquina, G.; Langer, J.; Sánchez-Costa, M.; Jiménez-Osés, G.; López-Gallego, F. Immobilization and Stabilization of an Engineered Acyltransferase for the Continuous Biosynthesis of Simvastatin in Packed-Bed Reactors. *ACS Sustain. Chem. Eng* **2022**, *10* (30), 9899-9910. DOI: 10.1021/acssuschemeng.2c02279.

(44) Zaak, H.; Siar, E.-H.; Kornecki, J. F.; Fernandez-Lopez, L.; Pedrero, S. G.; Virgen-Ortíz, J. J.; Fernandez-Lafuente, R. Effect of immobilization rate and enzyme crowding on enzyme stability under different conditions. The case of lipase from Thermomyces lanuginosus immobilized on octyl agarose beads. *Process Biochemistry* **2017**, *56*, 117-123. DOI: https://doi.org/10.1016/j.procbio.2017.02.024.